PROCEEDINGS OF SCIENCE

Measurement of inelastic hadronic cross sections in space with DAMPE

Paul Coppin[a,*] for the DAMPE collaboration

[a] *Department of Nuclear and Particle Physics, University of Geneva, CH-1211 Geneva, Switzerland*

E-mail: paul.coppin@cern.ch, paulcppn@gmail.com

The Dark Matter Particle Explorer (DAMPE) is an ongoing space-borne experiment for the direct detection of cosmic rays (CR). Thanks to its large geometric acceptance and thick calorimeter, DAMPE is able to detect CR ions up to unprecedented energies of hundreds of TeV. Following more than 8 years of successful operation, DAMPE has amassed a large dataset of high-energy hadronic interactions in a regime that is often difficult to probe by accelerator experiments. In this contribution, we show how DAMPE data can be used to measure inelastic ion-nucleon cross sections, and present a cross section measurement of both proton and helium on the BGO calorimeter. Phenomenological models are used to scale and compare our measurements to existing accelerator data and other experimental results.

42nd International Conference on High Energy Physics (ICHEP2024)
18-24 July 2024
Prague, Czech Republic

*Speaker

PoS(ICHEP2024)664

1. Introduction

The precise measurement of cosmic-ray (CR) nuclei fluxes requires an accurate knowledge of inelastic hadronic cross sections. A new energy frontier has been probed by the CALorimetric Electron Telescope (CALET) and the DArk Matter Particle Explorer (DAMPE) experiments, which have extended direct flux measurements of CR nuclei above the 100 TeV threshold. However, the uncertainty on these measurements is limited, at low and high energies alike, by our knowledge of hadronic models. In particular, inelastic cross sections present an important systematic, as they affect the effective acceptance and, therefore, the normalisation of CR nuclei fluxes. An inelastic cross section measurement of proton and ^{4}He is described in this contribution, as presented at the 42$^{\text{nd}}$ International Conference on High Energy Physics (ICHEP) and described in more detail in [1].

2. The Dark Matter Particle Explorer

DAMPE, short for Dark Matter Particle Explorer, is a satellite-based experiment. It orbits the Earth at an altitude of 500 km, and has a payload designed for the detection of CR electrons, photons, and hadronic nuclei [2, 3]. The payload consists of four distinct subdetectors, the:

- Plastic Scintillator Detector (PSD), which consists of 82 scintillating bars, placed in two double orthogonal layers, that enable measuring the charge of the primary particle [4–7];
- Silicon-Tungsten tracKer converter (STK), to accurately measure the track of the primary particle and promote the conversion of photons into electron-positron pairs [8–11];
- Bismuth-Germanium-Oxide (BGO) calorimeter, a one ton electromagnetic calorimeter made up of 14 orthogonal layers, with 22 bars of dimension $25 \times 25 \times 600$ mm^3 per layer [12–14];
- NeUtron Detector (NUD), which can measure the neutron content of showers, aiding the differentiation of electromagnetic and hadronic showers [15].

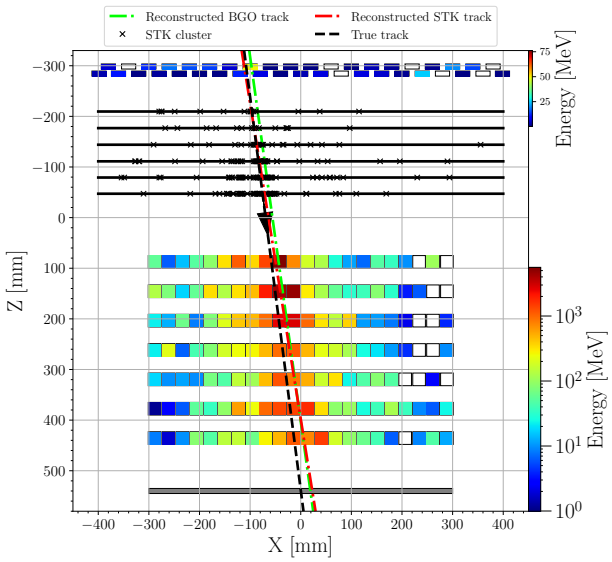

Figure 1: Visualisation in the xz-plane of a proton particle interacting with the DAMPE experiment from Geant4 simulations. From top to bottom, the three subdetectors shown are the PSD, STK, BGO, and NUD.

3. Data and Simulation

Data. The analysis presented in this work uses 88 months of data from the PSD, STK, and BGO sub-detectors; collected between May 2016 and September 2023.

Simulation. Proton and helium-4 particles were simulated in a kinetic energy range from 1 GeV to 100 TeV. The initial position and direction was chosen such that their trajectories represent a uniform flux from a hemispherical surface. Simulated events were weighted such that their energy distribution dN/dE matches that of the proton and helium flux measured by DAMPE [16–18]. Geant4 [19–21] with the FTFP-BERT physics list is chosen as the default simulation framework due to its good agreement with results from beam tests [7, 13, 22, 23]. To study the systematic uncertainty due to the assumed hadronic model, simulations were also performed with FLUKA in the same energy range [24, 25]

Event selection. A event selection is applied to proton and helium-4 primaries that interact inside the calorimeter. The selection starts by triggering on events which deposit an energy equal or higher than that of a minimum-ionising particle (MIP) in the top and bottom of the calorimeter [26]. Containment cuts are applied on the primary track to ensure that the trajectory is fiducially contained in the PSD, STK, and BGO subdetector [27]. The few percent background from leptons is rejected using a hadron-lepton variable developed in earlier work [28]. Finally, events are removed if their STK signal indicates that they interact before the calorimeter. Figure 2 shows in its left panel the median STK charge of the selected events, with vertical red lines indicating the charge window used to selection proton and helium.

Energy dependence. To enable measuring cross sections as a function of energy, the selected events are binned based on the total energy that they deposit in the calorimeter. The corresponding true kinetic energy distribution of each bin is shown in the right panel of Fig. 2, with the legend indicating the deposited charge range. The peak and width these distributions, obtained by fitting a langaus function, are used as the reference energy and uncertainty for each bin.

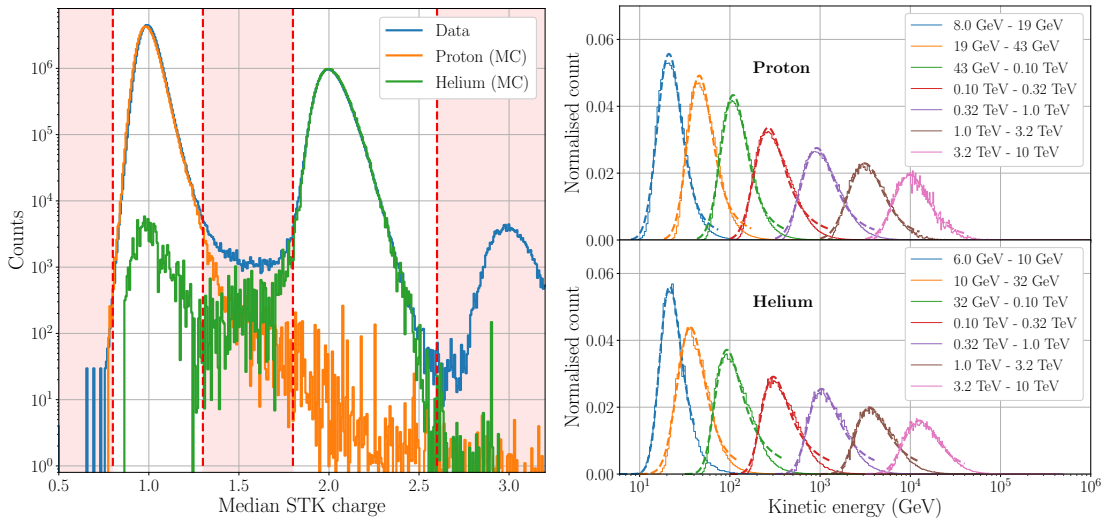

Figure 2: Left: Median charge observed in the STK subdetector after applying the analysis selection. Right: Distribution of the true kinetic energy, for events simulated with Geant4 in different bins of total BGO energy.

4. Analysis Procedure

Methodology. The inelastic cross section determines the distribution dN/dz of the number of primary particles N that interact inelastically as a function of depth z in the detector. dN/z deviates from a simply exponential decay primarily due to the energy and angular dependence of the effective acceptance after the analysis cuts. The cross section measurement in this work proceeds by measuring the distribution dN/dz of data and then tuning the cross section in simulation until its distribution best matches data. Rather than measuring a continuous function, the layered design of the BGO calorimeter instead favours a discrete classification. 16 categories are used. One for events which interact prior to reaching calorimeter, one for each of the 14 layers of the calorimeter, and one for events which pass the BGO without interaction.

Interaction depth classifier. The depth at which events interact inelastically is classified using an Extreme Gradient Boosting (XGB) classifier [29]. 70 input variables are provided to the classifier, primarily among which the energy and energy spread per BGO layer. After training the classifier is observed to have an accuracy $\geq 80\%$ for proton and helium-4 events simulated with both Geant4 and FLUKA.

Likelihood analysis. Agreement between the dN/dE distribution of data and MC is quantified using the following likelihood function

$$\mathcal{L} = \frac{N_{tot}!}{N_2!N_3!\cdots N_{10}!}\prod_{i=2}^{10}\alpha_i^{N_i} \ . \tag{1}$$

In this expression N_i for i from 2 to 9 is the number of events in data that interact in the i^{th} BGO layer, while N_{10} is the number of events in data that interact after the 9^{th} layer. Event interacting in the first BGO layer are excluded from the analysis due to expected reduced accuracy of the classifier for this class. The variable $\alpha_i \equiv N_i^{MC}/\sum_{j=2}^{10} N_j^{MC}$ represents the expected fraction of events in each subclass based on MC. By varying the cross section of the simulated events, the cross section value is determined as that which minimises the likelihood. This measurement is performed separately for each of the energy bins shown in the right panel of Fig. 2.

Uncertainties. Statistical uncertainties are determined by varying the observed values of N_i assuming binomials error, and then performing 10.000 pseudo-experiments. Systematic uncertainties arise from the: interaction depth classier, input spectrum used to weight MC, event selection, MC framework, assumed contribution of quasi-elastic scattering, and the calibrated energy scale of BGO. In the low energy bins, the total systematic error is at the few percent level, increasing to $5-10\%$ in the last 3 energy bins.

5. Results

Inelastic cross sections Figure 3 shows the results for proton (left) and helium-4 (right). In the case of proton we find that model predictions slightly overshoot the measured cross section at higher energies, indication a potentially lower overall normalisation. In the case of helium-4, our measurements are in good agreement with EPOS LHC [30, 31], QGSJetII-04, and DPMJET-III [32–34]; but are in tension with the Glauber model [35].

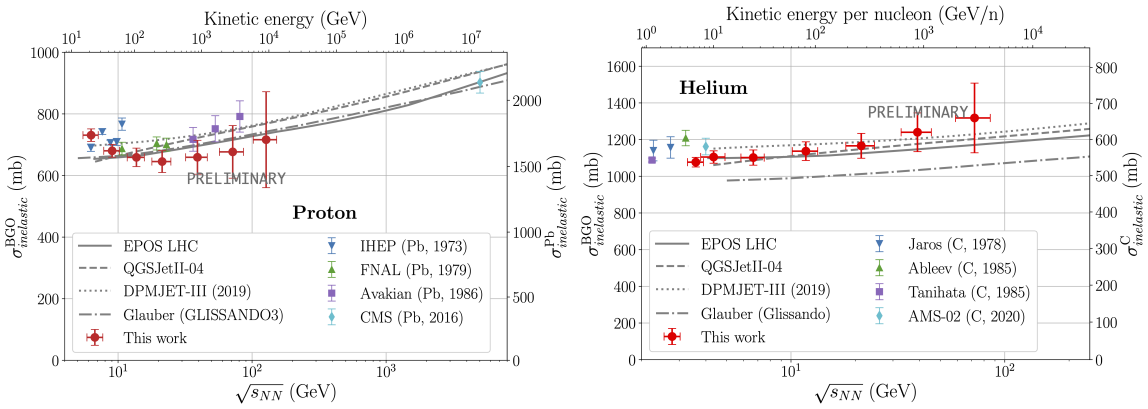

Figure 3: Left: Results of the inelastic cross section measurement of proton on $Bi_4Ge_3O_{12}$, compared to results from ground-based accelerator experiments [36–39] for proton-lead. The scaling between the two y-axes is derived using the EPOS LHC model. Aside from EPOS LHC [30, 31], the QGSJetII-04, DPMJET-III [32–34], and Glauber [35] model are also shown for comparison. Error bars include the statistical and systematic error. Right: Same as left figure, but showing the results for helium-4 nuclei, and comparing to measurements on a carbon-12 target [40–43].

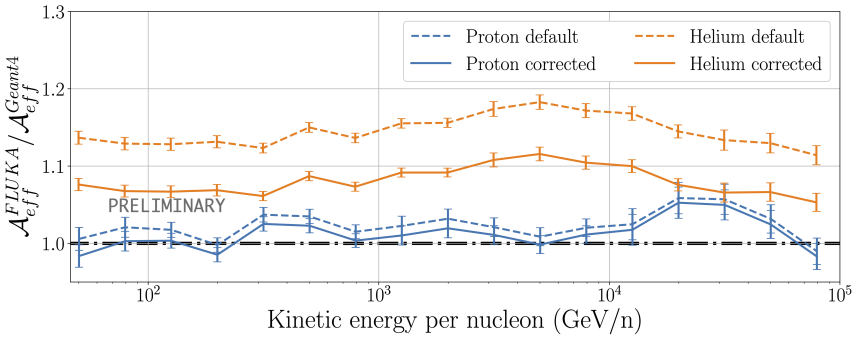

Figure 4: Acceptance ratio between FLUKA and Geant4 prior to any corrections (dashed line) and after correcting MC to the measured cross section (full line). After corrections the Geant4-FLUKA difference observed for helium-4 is reduced by half.

CR fluxes using corrected MC The cross sections measured in this work can be used to correct those of simulation frameworks such as Geant4 and FLUKA. Figure 4 shows a comparison of the effective detector acceptance $\mathcal{A}_{eff}$ in DAMPE analyses of the proton and helium flux. After applying a correction based on the cross section measurement, a significant improvement is observed between Geant4 & FLUKA.

6. Conclusions & Outlook

A measurement of the inelastic cross section of proton and helium-4 on a $Bi_4Ge_3O_{12}$ target has been presented. In the case of helium-4 these are the first measurement on any a heavy target material above 10 GeV/n. It has been shown that using these results can significantly reduce the systematic uncertainties of CR ion fluxes by increasing the accuracy of hadronic models, particularly in the case of helium-4. For further details, we refer the reader to [1].

References

[1] DAMPE Collaboration, arXiv:2408.17224. forthcoming.
[2] DAMPE Collaboration, *Astropart. Phys.* **95** (2017) 6–24.
[3] DAMPE Collaboration, *Astropart. Phys.* **106** (2019) 18–34.
[4] Y. Yu et al., *Astropart. Phys.* **94** (2017) 1–10.
[5] T. Dong et al., *Astropart. Phys.* **105** (Feb., 2019) 31–36.
[6] M. Ding et al., *Res. Astron. Astrophys.* **19** (mar, 2019) 047.
[7] Y. Zhang et al., *Nucl. Instrum. Methods Phys. Res. A* **953** (2020) 163139.
[8] A. Tykhonov et al., *Nucl. Instrum. Methods Phys. Res. A* **924** (2019) 309–315.
[9] A. Tykhonov et al., *Nucl. Instrum. Methods Phys. Res. A* **893** (2018) 43–56.
[10] P. Azzarello et al., *Nucl. Instrum. Methods Phys. Res. A* **831** (2016) 378–384.
[11] A. Tykhonov, V. Gallo, X. Wu, and S. Zimmer, *J. Phys.: Conf. Ser.* **898** (oct, 2017) 042031.
[12] Z. Zhang et al., *Nucl. Instrum. Methods Phys. Res. A* **836** (Nov., 2016) 98–104.
[13] Y. Wei et al., *Nucl. Instrum. Methods Phys. Res. A* **922** (2019) 177–184.
[14] Y.-L. Zhang et al., *Chin. Phys. C* **36** (jan, 2012) 71.
[15] Y.-Y. Huang et al., *Res. Astron. Astrophys.* **20** (sep, 2020) 153.
[16] F. Alemanno et al., *Phys. Rev. Lett.* **126** (May, 2021) 201102.
[17] Q. An et al., *Sci. Adv.* **5** (2019) eaax3793.
[18] A. Ruina et al., *PoS* **ICRC2023** (2023) 170.
[19] S. Agostinelli et al., *Nucl. Instrum. Methods Phys. Res. A* **506** (2003) 250–303.
[20] J. Allison et al., *IEEE Trans. Nucl. Sci.* **53** (2006) 270–278.
[21] J. Allison et al., *Nucl. Instrum. Methods Phys. Res. A* **835** (2016) 186–225.
[22] Z.-F. Chen et al., *Nucl. Instrum. Methods Phys. Res. A* **1055** (2023) 168470.
[23] W. Jiang et al., *Chin. Phys. Lett.* **37** (nov, 2020) 119601.
[24] T. Böhlen et al., *Nuclear Data Sheets* **120** (2014) 211–214.
[25] A. Fassò et al., *CERN, Technical report: INFN/TC_05/11, SLAC-R-77* (Oct., 2005).
[26] Y.-Q. Zhang et al., *Res. Astron. Astrophys.* **19** (sep, 2019) 123.
[27] A. Tykhonov et al., *Astropart. Phys.* **146** (2023) 102795.
[28] DAMPE Collaboration, *Nature* **552** (2017) 63–66.
[29] T. Chen et al. in *Proc. 22nd ACM SIGKDD Int. Conf. Knowl. Discov. Data Min.*, p. 785–794, 2016.
[30] K. Werner, *Nucl. Phys. B Proc. Suppl.* **175-176** (2008) 81–87.
[31] T. Pierog et al., *Phys. Rev. C* **92** (Sep, 2015) 034906.
[32] R. Engel, *Z. Phys. C* **66** (1995) 203–214.
[33] S. Roesler et al. in *Int. Conf. Adv. Monte Carlo Radiat. Phys. Part. Transp. Simul. Appl.*, pp. 1033–1038, 12, 2000.
[34] A. Fedynitch. PhD thesis, KIT, Karlsruhe, Dept. Phys., 11, 2015.
[35] P. Bożek et al., *Comput. Phys. Commun.* **245** (Dec., 2019) 106850.
[36] S. Denisov et al., *Nucl. Phys. B* **61** (1973) 62–76.
[37] A. Carroll et al., *Phys. Lett. B* **80** (1979) 319–322.
[38] V. V. Avakian et al., *Bull. Russ. Acad. Sci. Phys.* **50N11** (1986) 4–7.
[39] CMS Collaboration, *Phys. Lett. B* **759** (2016) 641–662.
[40] J. Jaros et al., *Phys. Rev. C* **18** (Nov, 1978) 2273–2292.
[41] V. G. Ableev, V. A. Bodyagin, and R. Dymarz, *Acta Phys. Polon. B* **16** (1985) 913–929.
[42] I. Tanihata et al., *Phys. Lett. B* **160** (1985) 380–384.
[43] Q. Yan, V. Choutko, A. Oliva, and M. Paniccia, *Nucl. Phys. A* **996** (2020) 121712.